Journal of Enzyme Inhibition and Medicinal Chemistry

http://informahealthcare.com/enz
ISSN: 1475-6366 (print), 1475-6374 (electronic)

J Enzyme Inhib Med Chem, Early Online: 1–11
 DOI: 10.3109/14756366.2015.1076811

Taylor & Francis
Taylor & Francis Group

RESEARCH ARTICLE

Exploring the biological consequences of conformational changes in aspartame models containing constrained analogues of phenylalanine

Adriano Mollica[1], Sako Mirzaie[2], Roberto Costante[1], Simone Carradori[1], Giorgia Macedonio[1], Azzurra Stefanucci[3], Szabolcs Dvoracsko[4], and Ettore Novellino[5]

[1]Dipartimento di Farmacia, Università di Chieti-Pescara "G. d'Annunzio", Chieti, Italy, [2]Department of Biochemistry, Sanandaj Branch, Islamic Azad University, Sanandaj, Iran, [3]Dipartimento di Chimica, Sapienza Università di Roma, Rome, Italy, [4]Institute of Biochemistry, Biological Research Centre, Hungarian Academy of Sciences, Temesvari krt, Hungary, and [5]Dipartimento di Farmacia, Università di Napoli "Federico II", Naples, Italy

Abstract

The dipeptide aspartame (Asp-Phe-OMe) is a sweetener widely used in replacement of sucrose by food industry. 2′,6′-Dimethyltyrosine (DMT) and 2′,6′-dimethylphenylalanine (DMP) are two synthetic phenylalanine-constrained analogues, with a limited freedom in χ-space due to the presence of methyl groups in position 2′,6′ of the aromatic ring. These residues have shown to increase the activity of opioid peptides, such as endomorphins improving the binding to the opioid receptors. In this work, DMT and DMP have been synthesized following a diketopiperazine-mediated route and the corresponding aspartame derivatives (Asp-DMT-OMe and Asp-DMP-OMe) have been evaluated *in vivo* and *in silico* for their activity as synthetic sweeteners.

Keywords

Aspartame, computational methods, 2′,6′-dimethyltyrosine, 2′,6′-dimethylphenylalanine, sweetener, T1R2 receptor

History

Received 29 May 2015
Accepted 16 July 2015
Published online 24 August 2015

Introduction

The low-calorie sweetener aspartame, namely aspartyl-phenylalanine methyl ester, is a common synthetic dipeptide ester which possesses a sweetening power around 200 times sweeter than sucrose. Considering its commercial importance in food industry, its safety has been widely investigated by studies in several human subpopulations, including healthy people, obeses, diabetics, etc. and its massive use has been recently criticized basing on a theoretical toxicity of its metabolic components, namely aspartate, phenylalanine and methanol. Nonetheless, additional research has been carried out to understand the possible association between aspartame and headaches, seizures, behaviour, cognition, and mood as well as allergic-type reactions. The question about its safety remains still unresolved[1].

The detection of sweet-tasting compounds (carbohydrates and non-caloric sweeteners) is mediated by a heterodimeric receptor composed of two subunits, namely T1R2 and T1R3. Moreover, this receptor modulates glucose transporters and glucose homeostasis in other ''non-taste'' organs (gastrointestinal tract, pancreas, bladder, adipose tissues, and brain) demonstrating to show a potential as new therapeutic target[2,3]. Small molecule inhibitors of sweet receptors have been demonstrated to reduce glucose absorption and calorie uptake providing an alternative strategy for the treatment of obesity and its related diseases.

Several structure–activity relationship studies have been conducted on aspartame derivatives[4–6], but none of them have explored the importance of the side chains orientation of the phenylalanine residue in influencing the sweet potency and the taste quality. It is well known that the incorporation of unnatural amino acids into bioactive peptides may lead to unique analogues, biologically more active and/or more selective than the parent peptides[7]. This is the result of strong modifications on the stereoelectronic properties of the peptide and of the secondary structure, as the stabilization of a folded conformation. Lately, it has been proved that the arrangements of the side chains of the residues are also important for the binding with the target molecules. For example, the introduction of 2′,6′-dimethyltyrosine (DMT) in place of the native Tyr[1] in endomorphin-1 yields a very potent analogue at the μ opioid receptor and a similar effect has been reported for the incorporation of 2′,6′-dimethylphenylalanine (DMP) in place of *C*-terminus Phe[8,9]. This behaviour can be explained with the concept of χ space[10–12]. In fact, side chains of natural amino acids possess a certain degree of flexibility around the χ dihedral angles, which allows the peptide to adapt its overall 3D shape to different receptors. In order to enhance potency and efficacy, the side chain's freedom of the native residue may be reduced in order to obtain a more favourable topology. Plotting energy versus χ dihedral angle is available in the Supplemental material. Considering the recent applications of this approach in peptidomimetics design[13,14], in this paper, we synthesized two new aspartame models in which the native phenylalanine residue was substituted by two constrained aromatic surrogates, namely 2′,6′-dimethyltyrosine and 2′,6′-dimethylphenylalanine.

In 2010, an effort was done to elucidate the molecular mechanism of the sweet taste enhancers. Umami and sweet taste receptors share a T1R3 subunit as a common subunit. It has been

Address for correspondence: Adriano Mollica, Dipartimento di Farmacia, Università di Chieti-Pescara ''G. d'Annunzio'', Via dei Vestini 31, 66100 Chieti, Italy. E-mail: a.mollica@unich.it

shown that the sweet enhancers have no effect on umami taste receptor. So, they probably bind to the *N*-terminal extracellular domain of T1R2 subunit. This subunit is composed of two distinct domains, Venus flytrap (VFT) and transmembrane domain, as present in T1R family receptors. Generation of hybrid receptors showed that the interaction mode of some enhancers is mediated by VFT domain of T1R2 subunit[15]. As a consequence, bioactivity and *in silico* evaluation of the binding mode of both derivatives have been explored using an established receptor model.

Materials and methods

Chemistry

The structure of the intermediates and the final compounds was confirmed by ^{1}H NMR spectra recorded on a 300 MHz Varian Inova spectrometer (Varian Inc., Palo Alto, CA). Chemical shifts are reported in parts per million (δ) downfield from the internal standard tetramethylsilane (Me_4Si). Homogeneity was confirmed by TLC on silica gel Merck 60 F254 (Merck, Darmstadt, Germany). The HR ESI-MS experiments were performed on a Thermo Scientific Q Exactive (Thermo Fisher Scientific, San Jose, CA). The MS was operated in the positive mode. The parameters used were the following: capillary temperature 220 °C, spray voltage 2.3 kV, and sheath gas 5 units.

Solutions were routinely dried over anhydrous Na_2SO_4 prior to evaporation. Chromatographic purifications were performed for the intermediate products by Merck 60, 70–230 mesh silica gel column and for the final products **4a** and **4b** by RP-HPLC. All chemicals used were of the highest purity commercially available.

All dipeptides were synthesized by solution phase peptide synthesis (SPPS) using Boc strategy following well-established procedures[16]. N^{α}-Boc deprotection was carried out by TFA treatment. DMP (**1a**) and DMT (**1b**) were synthesized following the method developed by Mollica and Costante (Patent Application ''Sintesi enantioselettiva di amminoacidi aromatici non-naturali'', Application Number: RM2015A000091, date: 27/02/2015) and transformed in methyl ester hydrochlorides **2a** and **2b** by treatment with $SOCl_2$ in MeOH, and used without further purification for the next step[16b] (Scheme 1).

Boc-Asp(*t*Bu)-DMP-OMe (3a)

Boc-DMP-OH (**1a**) was dissolved in MeOH, then $SOCl_2$ (2 eq.) was added dropwise at 0 °C. The mixture was allowed to warm to r.t. and stirred for 3 h, then the solvent was removed *in vacuo* to give HCl·H-DMP-OMe (**2a**) which was used for the next reaction without further purification. Coupling with Boc-Asp(*t*Bu)-OH was performed following the general coupling procedure. After silica gel chromatography using CH_2Cl_2/EtOAc (from 95:5 to 85:15) as eluent, the pure dipeptide was obtained as a colorless oil in 65% yield. HRMS calcd.: 478.2679, found: 478.2687. ^{1}H NMR ($CDCl_3$) δ: 7.11 (1H, d, DMP NH), 7.05–6.97 (3H, m, Ar), 5.54 (1H, d, BocNH), 4.77–4.69 (1H, m, Asp αCH), 4.42–4.35 (1H, m, DMP αCH), 3.59 (3H, s, OMe), 3.08–2.87 (2H, m, DMP βCH_2), 2.84–2.51 (2H, m, Asp βCH_2), 2.34 (6H, s, DMP CH_3), 1.43, and 1.46 (18H, s, Boc, O*t*Bu).

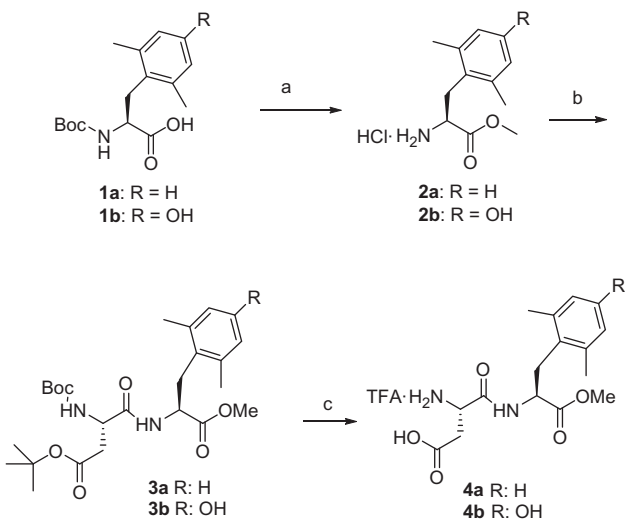

Scheme 1. (a) $SOCl_2$/MeOH, r.t., 3 h; (b) Boc-Asp(*t*Bu)-OH, EDC·HCl, HOBt, NMM, DMF, r.t., overnight; (c) TFA/CH_2Cl_2 1:1, r.t., 1 h, under N_2.

TFA·H-Asp-DMP-OMe (4a)

N^{α}-Boc and O*t*Bu deprotections of compound (**3a**) were performed as reported for TFA·H-Val-Gly-OMe. The crude product was purified by RP-HPLC semi-preparative C18 column (eluent: ACN/H_2O gradient, 5–80% over 20 min) and the TFA salt was obtained, after freeze drying, in quantitative yield as a white powder. HRMS calcd.: 322.1529, found: 322.1535. ^{1}H NMR (DMSO-d_6) δ: 8.98 (1H, d, DMP NH), 7.00–6.98 (3H, m, Ar), 4.86–4.60 (1H, m, Asp αCH), 4.09–4.05 (1H, m, DMP αCH), 3.50 (3H, s, OMe), 3.15–2.70 (4H, m, DMP βCH_2, Asp βCH_2), 2.52 (6H, s, DMP CH_3).

Boc-Asp(*t*Bu)-DMT-OMe (3b)

HCl·DMT-OMe (**2b**) and Boc-Asp(*t*Bu)-DMT-OMe (**3b**) were synthesized as reported for compound (**3a**) and, after column chromatographic purification, the dipeptide was obtained as a colourless oil in 85% yield. HRMS calcd.: 494.2628, found: 494.2640. ^{1}H NMR ($CDCl_3$) δ: 7.88 (1H, d, DMT NH), 6.50 (2H, s, Ar), 5.46 (1H, d, BocNH), 4.68–4.55 (1H, m, Asp αCH), 4.32–4.25 (1H, m, DMT αCH), 3.64 (3H, s, OMe), 3.40–2.21 (2H, m, DMT βCH_2), 2.92–2.56 (2H, m, Asp βCH_2), 2.28 (6H, s, DMT CH_3), 1.44, and 1.42 (18H, s, Boc, O*t*Bu).

TFA H-Asp-DMT-OMe (4b)

N^{α}-Boc and O*t*Bu deprotections of compound (**3b**) were performed as reported for compound **3a**. The crude product was purified by RP-HPLC semi-preparative C18 column (eluent: ACN/H_2O gradient, 5–80% over 20 min) and the TFA salt was obtained in quantitative yield as a white powder after freeze drying. HRMS Calcd.: 338.1478, found: 338.1489. ^{1}H NMR (DMSO-d_6) δ: 9.14 (1H, s, DMT OH), 8.84 (1H, d, DMT NH), 6.40 (2H, s, Ar), 4.56–4.41 (1H, m, Asp αCH), 4.10–3.96 (1H, m, DMT αCH), 3.53 (3H, s, OMe), 3.15–2.56 (4H, m, DMT βCH_2, Asp βCH_2), 2.12 (6H, s, DMT CH_3).

NMR conformational studies

To gain further information on the preferred conformation of the models, we examined the 2D ROESY ^{1}H NMR of aspartame and [DMP^2]aspartame. As shown in Table 1 and Figure 1, aspartame and [DMP^2]aspartame derivatives show strong sequential NOEs Phe NH–Phe CH$^{\alpha}$. This effect can be observed for both products. Some differences can be appreciated in the NOEs between the aromatic ring protons and the backbone of the peptides of aspartame, and the NOEs between the Ar–CH_3 protons and the backbone of the [DMP^2]aspartame. These data strongly suggest that the aromatic ring of the DMP model is restricted into a well-defined χ angles, according to the computational energy calculation. All 1D and 2D ^{1}H NMR experiments were performed at 300 MHz on a Varian Inova NMR spectrometer (Varian, Palo Alto, CA) with a constant temperature at 298 K. The ROESY spectra were obtained using standard pulse programs, with a

Table 1. Observed NOE Cross Peaks and intensities of aspartame and [DMP^2]aspartame in DMSO-d_6 and J coupling constants (Hz)[a].

	Aspartame	[DMP^2]aspartame	*J* coupling constants (Hz)
Asp NH_3^+—Asp CH^α	w	w	Aspartame
Asp NH_3^+—Phe CH_2^β	–	w	Phe NHJ = 7·8
Phe NH—aromatics	w	–	AB part of ABX system Phe:
Phe NH—Phe CH^α	m	m	$J_{ab} = 14$; $J_{ax} = 6$; $J_{bx} = 9.3$
Phe NH—Asp CH^α	s	s	AB part of ABX system Asp:
			$J_{ab} = 15$; $J_{ax} = 3.3$; $J_{bx} = 8.1$
Phe NH—Phe CH_2^β	–	m	DMP[aspartame]
Phe NH—Ar CH_3	–	w	DMP NHJ = 7·5
Phe CH^α—Asp CH_2^β	m	m	AB part of ABX system DMP:
Phe CH_2^β—aromatics	m	–	$J_{ab} = 14.1$; $J_{ax} = 8.1$; $J_{bx} = 6.9$
Ar CH_3—aromatics	–	s	AB part of ABX system Asp:
Ar CH_3—Phe CH^α	–	m	$J_{ab} = 17.4$; $J_{ax} = 3.3$; $J_{bx} = 8.1$
Ar CH_3—Phe CH_2^β	–	m	

[a]NOE intensities are classified as weak (1.6–5.0 Å), medium (1.6–3.6 Å), and strong (1.6–2.9 Å).

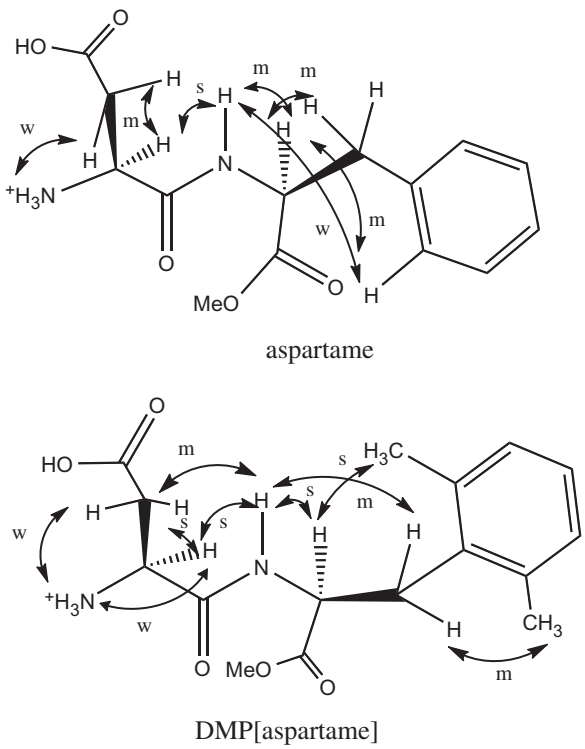

Figure 1. Relevant interproton correlations as deduced by ROESY experiments of aspartame and [DMP^2]aspartame.

mixing times of 300 ms, t1 = 1.5 s. The 2D NMR matrixes were created and analyzed using the Agilent WNMR computer program (Agilent Technologies Inc., Atlanta, GA). Each two-dimensional spectrum was acquired in a 1024 × 1024 data matrix complex points in F1 and F2. Zero filling in F1 and sine windows in both dimensions was applied before Fourier transformation. Chemical shifts (δ) are quoted in parts per million (ppm) downfield from tetramethylsilane, and values of coupling constants are given in Hz.

Sensory evaluation

Standard [DMT^2]aspartame and [DMP^2]aspartame were synthesized and tested as TFA salts as reported by Dörrich et al.[17] Qualitative taste assays were carried out following the protocol reported by the same author[17]. We conduct our studies in compliance with the principles of the Declaration of Helsinki. TFA·Aspartame, commercial aspartame, [DMT^2]aspartame and [DMP^2]aspartame were tasted by three volunteers in blind tests using diluted aqueous solutions of each test compound. Different concentrations (between 0.1 and 0.001% (w/v)) of each dipeptide were evaluated at 3–5 min intervals. About 1.5 mL of each solution was applied via pipettes and allowed to flow over the volunteer's tongue for 3 s and then washed out. Sweetness intensities were determined relative to aqueous sucrose solutions of 0.5, 2.0, 4.0, and 8.0% (w/v) as the reference. The [[DMT^2]aspartame and [DMP^2]aspartame solutions resulted to be tasteless even at the higher concentration. The absence of taste of the novel synthesized aspartame analogues was the object of the *in silico* investigation.

Computational experiments

Sequence alignment

Due to the lack of experimental data, a three-dimensional structure of sweet T1R family receptors, the 3D structure of extracellular VFT domain of T1R2 was constructed by homology modelling (Figure 2). In the first stage, the amino acid sequence of human T1R2 was retrieved from Swiss–Prot database with the accession number Q8TE23. Then, the BLAST search engine from National Center for Biotechnology Information (NCBI) was utilized to find the suitable template with pdb format. Among the listed templates, crystal structure of the extracellular region of the group II metabotropic glutamate receptor complexed with L-glutamate (pdb code: 2E4U) with resolution 2.35 Å, was used as a template[18]. Alignment between query sequence and selected template was done by ClustalW2 from its website[19,20] with default parameters. Produced alignment, which showed 28% identity, was used for 3D model building.

T1R2 model building by homology modeling

To construct the T1R2 models, MODELLER 9v14 package (Andrej Sali Lab, San Francisco, CA) was employed. Using this package, one hundred models of human T1R2 were constructed and to select the best model, the one with the lowest value of Discrete Optimized Protein Energy (DOPE)[21] was picked. The final model was minimized by the steepest descent algorithm implemented in GROMACS 4.5 package[22]. The Ramachandran plots of models also were computed by PROCHECK to assess the psi and phi angles of model residues and clarify the model quality[23].

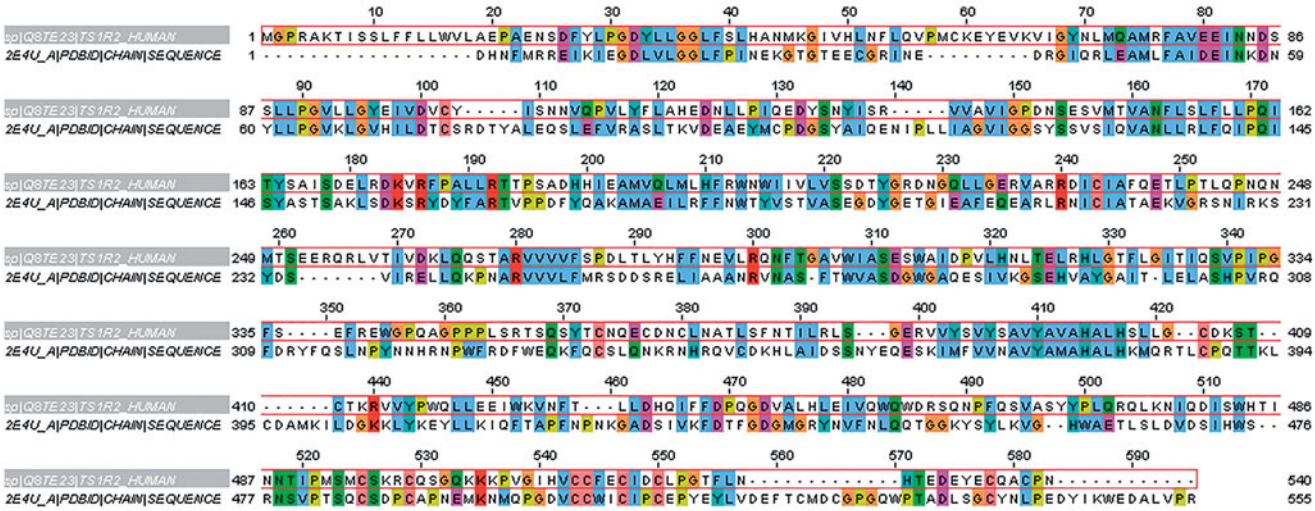

Figure 2. Sequence alignment of VFT domain of T1R2 with extracellular region of glutamate receptor (pdb code: 2E4U). Same color of residues shows the same properties. (Colors in this figure are referred to the web version of this article.)

Docking study of T1R2 model and ligands

To dock the aspartame, DMP and DMT into the binding site of T1R2 model, AutoDock Vina was employed[24]. This molecular docking software profits of knowledge-based potentials and empirical scoring functions[24,25]. To generate the 3D structures of ligands, PRODRG server was utilized[26]. After generation of 3D structures of aspartame, DMP and DMT, their non-polar hydrogen atoms were deleted and subsequently, Gasteiger–Marsili charges were assigned[27]. For protein preparation before docking study, Gasteiger–Marsili charges implemented in Autodock Tools 1.5.4 were allocated for T1R2 model. To assess the binding affinity of ligands to the T1R2 binding site, a box with a grid map with $30 \times 30 \times 30$ points and grid-point spacing of 1 Å was set up at the geometrical center of the residue Asp 278. For all docking runs, a default value of exhaustiveness parameter was assigned. All poses were re-clustered with x-score v1.1 and one with the highest average score was saved for further analysis and studies. The three scoring functions of X-score have been calibrated with a large training set of 800 protein–ligand complexes. Thus, it can be applied to a wider range of biomolecular systems giving more robust results[28].

Molecular dynamic simulations

Following the molecular docking, molecular dynamic (MD) simulations were done for T1R2, T1R2:aspartame, and T1R2:DMP complexes. All MD simulations were executed in periodic boundary conditions (PBC), using GROMOS96 43A1, a united atom force field, by GROMACS 4.5 package. To check the ionization state of ionizable residues, PROPKA 2.0 was used and the correct states were assigned for them[29]. GROMACS parameters of aspartame, DMP and DMT, were generated by PRODRG server[26]. To increase the precision in charge assignment, the atom charges of aspartame, DMP and DMT, were determined from the equivalent functional group in a GROMACS-building block file[30,31]. Eleven Na^+ counter ions were added to all systems to neutralize the negative charges. During the minimization, the protein non-hydrogen atoms were kept fixed in their initial configuration. After neutralization, all systems were introduced to the steepest descent minimization algorithm with an energy step size of 0.01. The minimization was converged when the maximum force was smaller than 10.0 kJ/mol. Successively, position restraint procedure was carried out in association with temperature coupling (NVT)[32] and pressure coupling (NPT) ensembles[33]. For each system, two coupling groups including protein (or protein ligand), solvent and ions were assigned. These groups were equilibrated separately at 300 K with a coupling constant of 0.1 ps and time duration of 100 ps. For NPT equilibration, a pressure of 1 bar, a time duration of 100 ps, and a time constant of 2 ps were allotted. In both ensembles mentioned above, PME method, with an interpolation order of 4, was used to compute the long-range electrostatic interactions[34]. LINCS algorithm was used to constrain covalent bond length[35]. The short-range neighbor list, short-range electrostatic, and short-range van der Waals cut-offs were set to 1.2 nm. For all MD runs, a 30 000 ps molecular dynamics was accomplished on the entire system. The trajectories were analyzed using the standard tools implemented in the GROMACS package.

Calculation of binding free energy

Modified Molecular Mechanics–Poisson Boltzmann Surface Area (MM-PBSA) method[35] was used to compute the interaction free energy between DMP and DMT with T1R2, separately. In this method, based on its theory, the free energy of binding can be expressed as follows:

$$\Delta G_{binding} = G_{complex} - \left(G_{protein} + G_{ligand}\right)$$

where $G_{complex}$ is the total free energy of the protein–ligand complex and $G_{protein}$ and G_{ligand} are total free energies of the separated form of protein and ligand in solvent, respectively. In our study, van der Waals, Electrostatic, Polar solvation, the solvent accessible surface area, solvent accessible volume y and Weeks–Chandler–Andersen energies were computed by *g_mmpbsa*[36].

Results and discussion

Chemistry

DMP and DMT have been synthesized following the method licensed by Mollica and Costante (patent titled ''Sintesi enantioselettiva di amminoacidi aromatici non-naturali'', Application Number: RM2015A000091, date: 27/02/2015) and their chemical–physics parameters were equal to those of the commercial products. Boc-DMP-OH and Boc-DMT-OH were converted into the corresponding methyl esters hydrochloride by

Table 2. Stereo-chemical quality of template and model checked by PROCHECK.

	Ramachandran plot quality (%)				Goodness factor		
PROCHECK	Core	Allowed	General	Disallowed	Dihedral	Covalent	Overall
Template (2E4U)	86.1	12.6	1.3	0	0.08	0.49	0.25
T1R2 model	87.1	10.4	1.6	0.9	−0.09	−0.28	−0.16

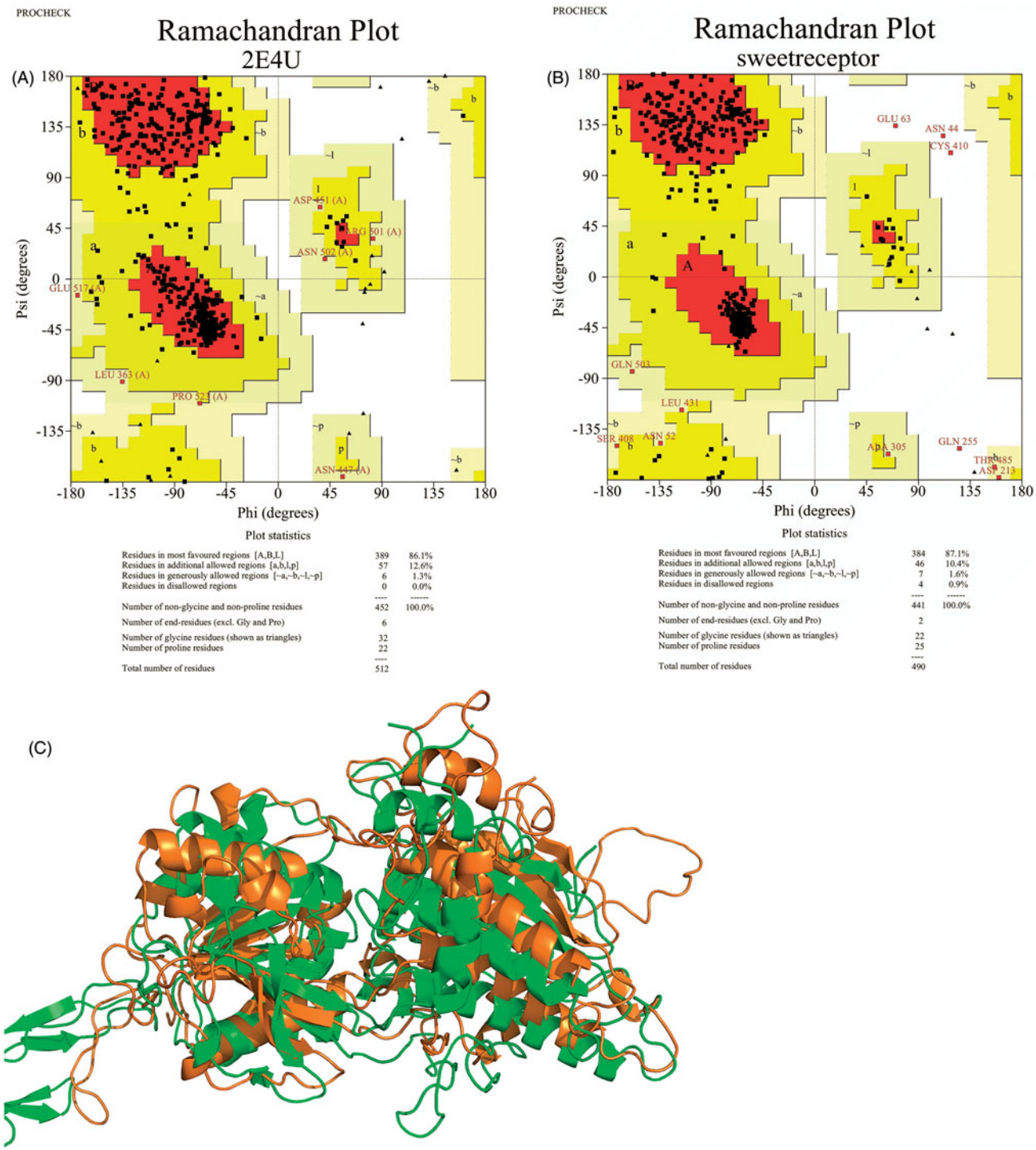

Figure 3. Ramachandran plot of template (2E4U) (A), TIR2 model (B), and cartoon view of superposition of template and TIR2 model (C). In the superimposed image, template and TIR2 model are shown in green and brown, respectively. (Colors in this figure are referred to the web version of this article.)

treatment with $SOCl_2$ in MeOH[16b,37]. The so obtained building blocks were coupled in the next step to Boc-Asp(O*t*bu)-OH. The protected aspartame derivatives were then purified by silica gel chromatography and deprotected by TFA in CH_2Cl_2. TFA salt were purified by RP-HPLC, C18 (ACN/H_2O, gradient, 1% TFA).

Computational modelling of T1R2

The VFT domain of T1R2 subunit was modeled by the homology modeling method to investigate the interaction mode of aspartame, DMP and DMT. Sequence alignment between VFT domain of T1R2 and the template (2E4U) is shown in Figure 1. The residues with same physicochemical properties are shown in same color. The selected template is an extracellular region of metabotropic glutamate receptor (mGluR)[18]. All mGluRs have also the *N*-terminal ligand-binding domain, which is often called the VFT module[38,39]. An agonist is included in the template pdb file, which can help to model the orientation of T1R2 active site. The best template selected by BLAST had just 28% identity. Because of low identity between the template and query sequence, validation of the generated 3D model is necessary to elucidate the model validity. Thus, the quality of the model was evaluated by PROCHECK.

As shown in Table 1, 86.1% of template residues are located in favored core regions with no one in disallowed region. For our model, in comparison with the template, a bit more residues are located in core regions (87.1) with a relatively low percentage of residues 1.3% in generously allowed regions and 0.9% in disallowed regions. For acceptable structures, it is expected that more than 85% of residues fall into the core regions. The second

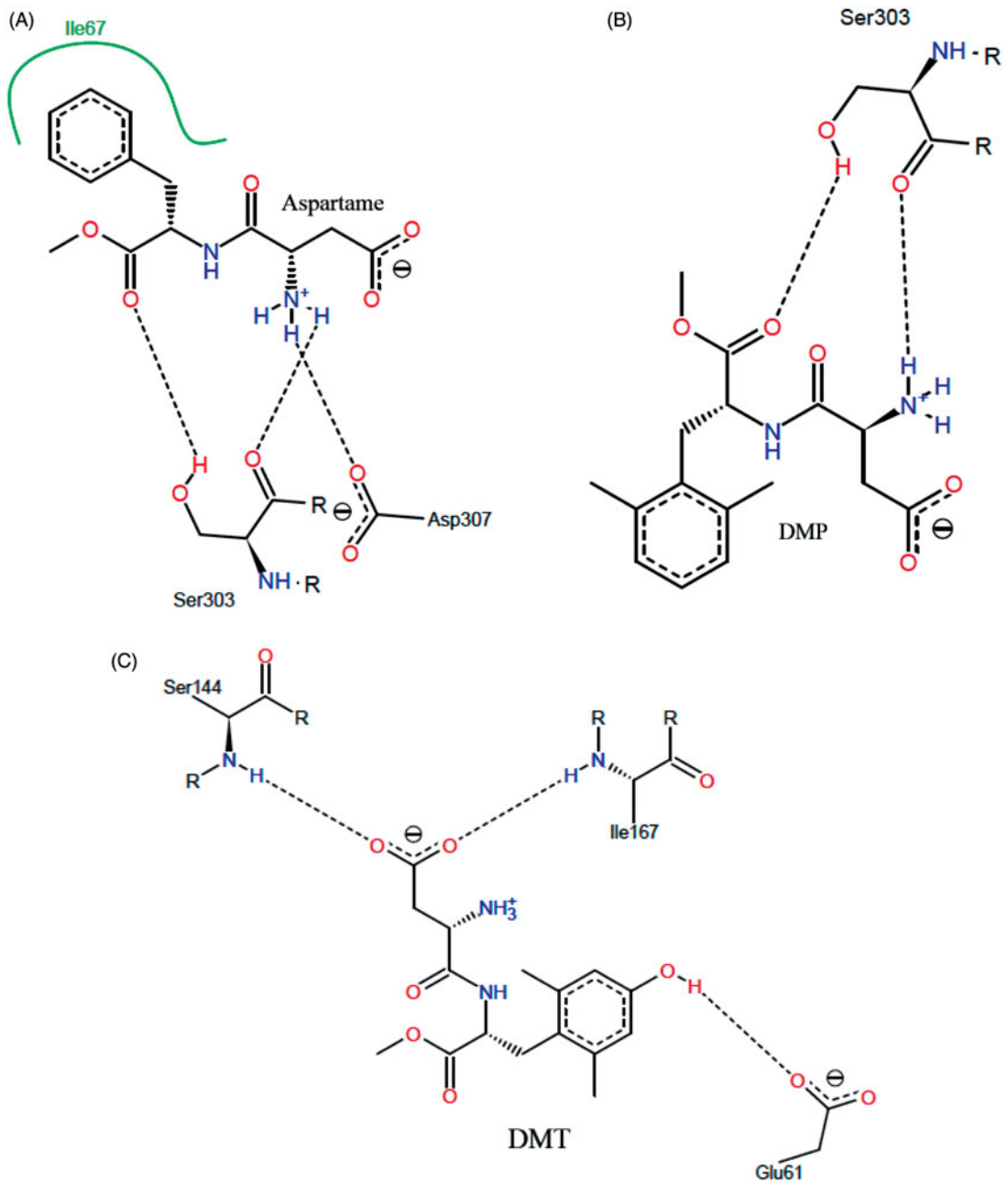

Figure 4. (A) Schematic two-dimensional representations of the binding interactions between aspartame and binding site of T1R2 model. Black dashed lines are hydrogen bonds. Hydrophobic interactions are shown by green solid line; (B) schematic two-dimensional representations of the binding interactions between DMP and binding site of T1R2 model. Black dashed lines are hydrogen bonds; (C) schematic two-dimensional representations of the binding interactions between DMT and binding site of T1R2 model. Black dashed lines are hydrogen bonds. (Colors in this figure are referred to the web version of this article.)

set of parameters, Goodness factor, was evaluated and summarized in Table 2. Reasonable values of G-factor in PROCHECK are between 0 and −0.5 with the best models exhibiting values close to zero[40]. The overall G-factor for TIR2 model (−0.16) shows a good and acceptable quality.

Ramachandran plots of template and T1R2 model are shown in Figure 3(A) and (B), respectively. As seen in Figure 3(B), 97.5% of T1R2 model residues were either in the most-favored regions or the additionally allowed regions. Moreover, Figure 3(C) shows the superposition of the template and T1R2 model. The most conformational differences between the template and T1R2 are related to loops.

Molecular docking analysis

Molecular docking of aspartame, DMP and DMT, was performed to evaluate the potential binding modes of the three peptide derivatives. The docking results were clustered and screened based on the algorithm of binding energy calculation implemented in AutoDock Vina. Figure 4(A) shows the interaction mode between aspartame and T1R2 model. Within a hydrophobic pocket of T1R2, Ile67 forms a hydrophobic interaction with the phenyl moiety of aspartame. Also, hydroxyl and carbonyl moieties of Ser303 interact with carbonyl and amino groups of aspartame *via* hydrogen bonding, respectively. Carboxyl moiety of Asp307 can form a salt bridge with NH_3^+ of aspartame. In 2006, Cui et al., based on a homology modeling study, demonstrated that Asp307 and Ser303 are the main residues involved in interaction with aspartame, due to the formation of hydrogen bonding and salt bridging[41]. Zhang et al. showed that Lys65, Leu279, Asp278, and Asp307 of T1R2 interact with the enhancer SE-3[15]. It seems that the interaction mode of DMP with T1R2, in comparison with aspartame, is slightly different (Figure 4B). The bulkier aromatic ring of DMP prevents to form a hydrophobic interaction. Based on this behaviour, Ser303 interacts with DMP through hydrogen bonding. In contrast to aspartame and DMP, DMT binds to T1R2 with a completely different pattern. With regard to Figure 4(C), NH of Ser144 and Ile167 formed a hydrogen bond with the carboxyl moiety of DMT. An additional hydrogen bonding is formed between carboxyl moiety of Glu 61 and hydroxyl group of DMT. Based on our docking study, the only hydrophobic interaction of the binding site is present in T1R2:aspartame complex. For further analysis, aspartame and DMP were selected to perform MD simulation.

Molecular dynamic simulation

Protein folding, enzymatic reaction, molecular recognition, and substrate–receptor bonding take place as a result of inter and intra-molecular interactions between biomacromolecules and ligands. MD simulation of the biological process is a powerful tool to generate such information at the microscopic level. In this stage, MD simulations of free T1R2, T1R2:aspartame and T1R2:DMP complexes were done to demonstrate and elucidate the mode of interaction between peptides and T1R2 during 30 ps. In addition, binding free energy and receptor conformational changes in the absence and presence of peptides were investigated.

Root mean square deviation (RMSD)

To assess the equilibration of MD trajectories, RMSD is considered a crucial parameter. RMSD values of the backbone atoms of T1R2 are plotted as a function of time to verify the stability of each system during 20 ps MD simulation. The RMSD

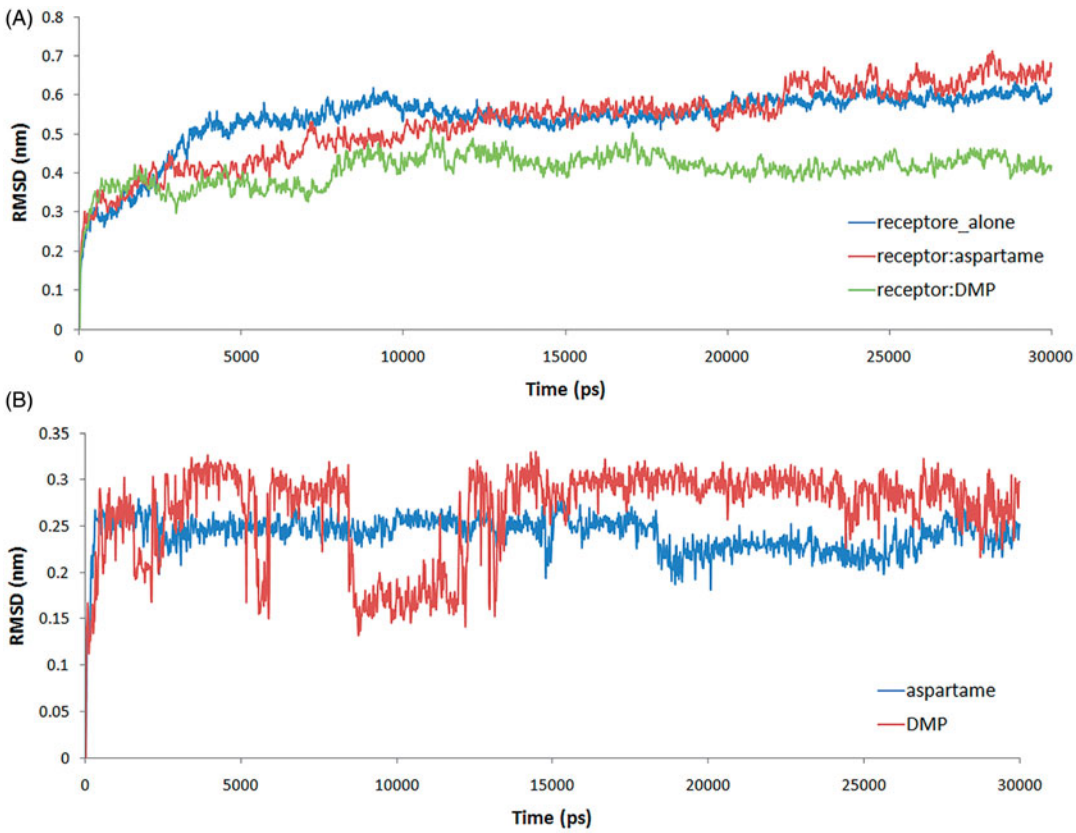

Figure 5. (A) RMSD values of T1R2:aspartame (red line), T1R2:MDP (green line), and free T1R2 (blue line) during MD simulation; (B) RMSD values of aspartame and DMP in binding site of T1R2 model. (Colors in this figure are referred to the web version of this article.)

values of free T1R2, T1R2:aspartame and T1R2:DMP complexes are shown in Figure 5(A). RMSD values of free T1R2 are increased up to 0.6 nm at 9100 ps. After a short decrease of RMSD to 0.53 nm, the system is equilibrated at the last 10 000 ps. In the case of T1R2:aspartame complex, RMSD is variable between 0.3 and 0.7 nm. Steady increase of RMSD is occurred till 21 700 ps. RMSD value for T1R2:DMP complex is between 0.2 and 0.48 nm. After increasing up to 0.44 nm at 7900 ps, the system approximately is equilibrated till 30 000 ps. It seems that binding of the DMP to T1R2 decreases the backbone flexibility of T1R2 and preserves it in a ''rigid state''. Conversely, binding of aspartame to T1R2 can promote some backbone flexibility, which may be necessary to form the active T1R2:T1R3 heterodimer. The RMSD values of aspartame and DMP to T1R2 model were acquired on the MD simulation of two systems to get information on position fluctuations. As shown in Figure 5(B), the RMSD of aspartame atoms rose to 0.26 nm after 300 ps and then leveled off to 0.25 nm. In the case of DMP, RMSD increased up to 0.3 nm, then a short decreasing to 0.15 nm is occurred and finally, the atoms were equilibrated approximately at the second half time of MD simulation. In comparison with DMP, aspartame has been reached to equilibrium more quickly.

Root mean square fluctuation (RMSF) and induced conformational changes

RMSF computation with respect to the average MD simulation conformation can be used to evaluate and assess the flexibility differences among residues. Figure 6 shows the backbone RMSF versus residue number. In Figure 6(A), RMSF of free T1R2 against T1R2:aspartame complex is depicted. In addition, RMSF of free T1R2 against T1R2:DMP complex is shown in Figure 6(B). VFT domain of T1R2 consists of two globular sub-domains joined by a three-stranded flexible hinge[14]. The first connection flexible strand is composed of Thr183, Thr184, Pro185, and Ser186 with RMSF values of 0.972, 1.093, 1.208, and 1.208 Å, respectively. These values approximately remained unchanged in T1R2:DMP complex (Figure 6B). In the case of T1R2:aspartame complex, these values are increased up to 1.156, 1.238, 1.405, and 1.412 Å (Figure 6A). The second strand is made of Ala445, Leu446, His447, and Leu448. These residues connect the two β-sheets belonging to sub-domains. Gly324, Ile325, Thr326, Ile327, and Gln328 form the third strand. Based on our data, RMSF of all three strand residues of T1R2:aspartame complex, in comparison with free T1R2 and T1R2:DMP complex, are increased. So, the mentioned ''hinge'' may have a critical role in T1R2 conformational changes and causes emerging the sweat taste response. Moreover, some researchers claimed that brazzein, a well-known sweet-tasting protein, binds to the ''hinge'' region of T1R2[42]. Previously, it has been shown that the ''hinge'' region of metabotropic glutamate receptors allows T1R2 conformational changes between open and closed conformations[43]. Sweet taste receptors have the highest similarity with metabotropic glutamate receptors in ''hinge'' region[15,42]. Thus, these ''open'' and ''close'' conformational changes can be true for our T1R2 model. Based on our MD simulations, binding of aspartame to

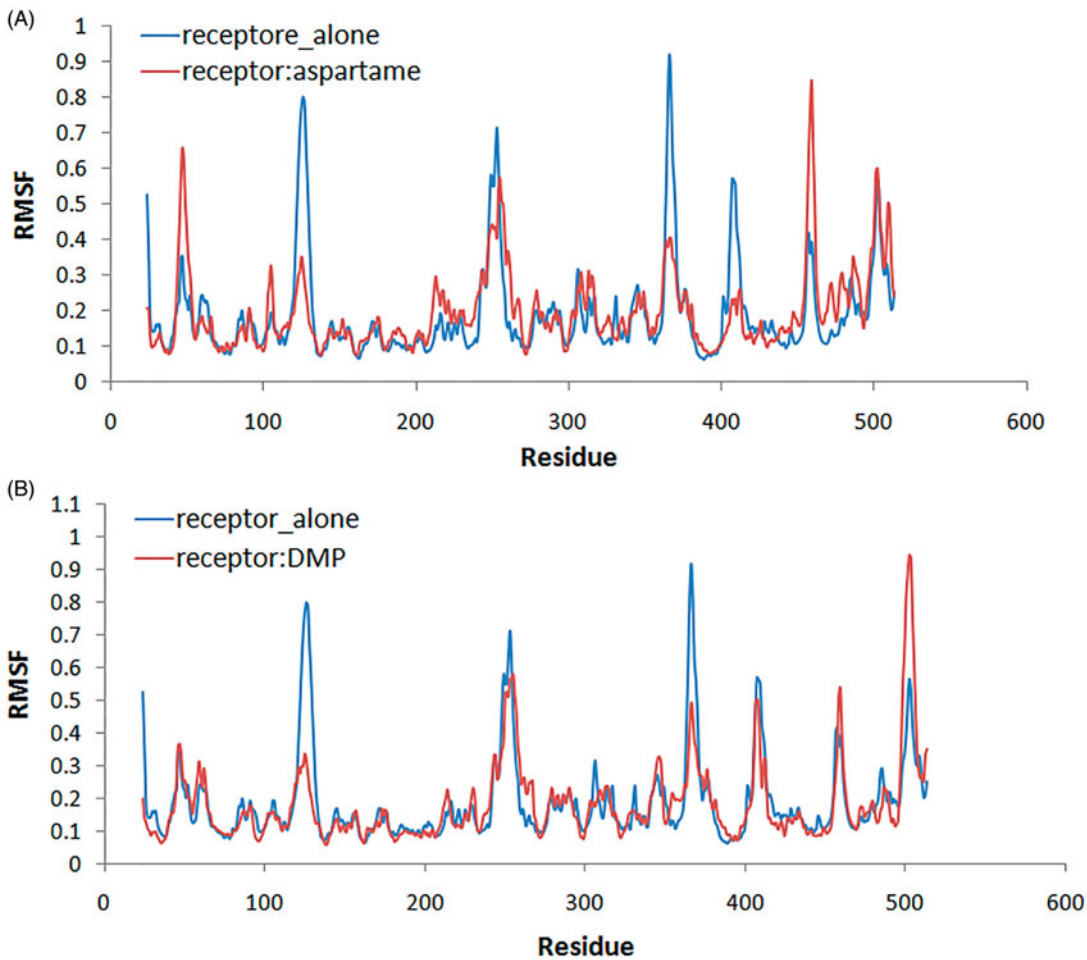

Figure 6. (A) RSM fluctuation of residues during MD simulation. RMSF comparison between free T1R2 (blue line) and T1R2:aspartame complex (red line); (B) RMSF comparison between free T1R2 (blue line) and T1R2:DMP complex (red line). (Colors in this figure are referred to the web version of this article.)

VFT domain triggers some conformational changes. As shown in Figure 7, side chain NH_3 of Lys60 from upper lobe interacts with backbone carbonyl moiety of Ile306 belonging to lower lobe via hydrogen bonding. This interaction can be inspected during 30 ns MD simulation. Figure 8 exhibits the distance between a nitrogen atom of Lys60 and oxygen of Ile306. For free T1R2, the distance is about 13 Å till 7.4 ns. Then, increased up to 24 Å and followed by a reduction to 14 Å. In the case of T1R2:aspartame complex, after a steady variation about 5.4 Å, it fell down to 2.9 Å. In an opposite manner, for T1R2:DMP complex, after a short fall between 11 and 15 ns, the distance increased up to approximately 29 Å. Due to binding of aspartame to the T1R2 model, a hydrogen bonding is formed between backbone carbonyl moiety of Ser165 and hydroxyl moiety of Thr184 (Figure 9A). In the presence of DMP in binding site of T1R2 model, these residues are too far to be able to interact to gather (Figure 9B).

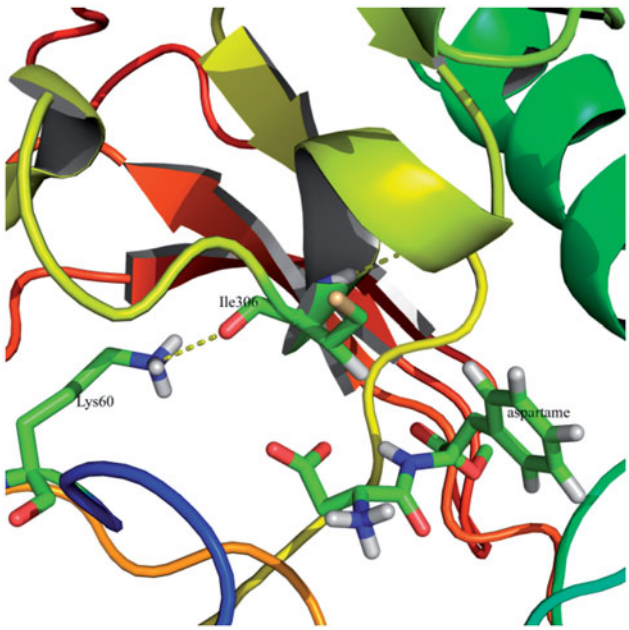

Figure 7. The computed binding mode of Lys60 with Ile306 in the binding site of T1R2 model. The hydrogen bonds are shown by the yellow dashed lines. (Colors in this figure are referred to the web version of this article.)

High-throughput MM-PBSA for binding free energy calculations

To estimate the interaction free energy between aspartame/DMP and VFT domain of the T1R2 model, MM-PBSA method was used[36]. Recently, a combination of MM-PBSA and molecular dynamic method has been used to re-score the docked poses. By applying this new method, the scoring function has been increased significantly[44–46]. The snapshots were extracted from the last 10 ns of MD trajectories for the analysis of the binding free energy. In Table 2, the binding free energy of aspartame and DMP to T1R2 model is −86.539 and −39.61, respectively. Based on our results, van der Waals energy is the most effective energy, which favors the binding of aspartame and DMP to binding site of T1R2 model. As shown in Table 3, binding of DMP, in comparison with aspartame, increases the van der Waals and electrostatic energies. Thus, increasing the hydrophobicity of aspartame opposes to the binding. This result suggests that the optimizations of van der Waals interactions between the agonists and T1R2 model may lead to the potent sweeteners.

Conclusion

Conformational constricted amino acids are important tools to explore the topographical preferences of bioactive peptides. DMP and DMT, in particular, have been recently used in the field of opioid peptides together with Δ^zPhe and other constrained residues with remarkable results[11]. Using our recent developed method to gain access to DMT and DMP and their *N*- or *C*-terminal protected derivatives, we have incorporated these two amino acids as phenylalanine surrogates in aspartame. The effects of this approach on the sweetener power have been evaluated. Our

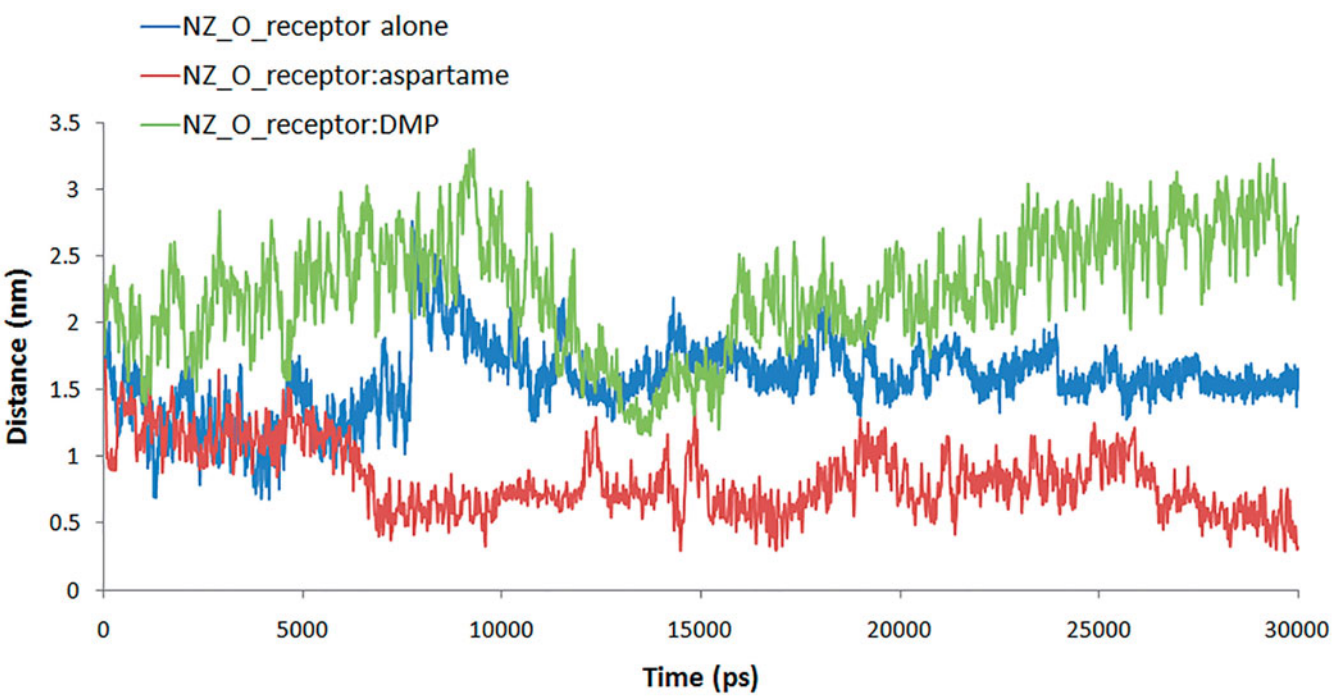

Figure 8. Distance changes between nitrogen atom of Lys60 and oxygen of Ile306 in free T1R2 (blue line), T1R2:aspartame (red line) and T1R2:DMP complexes (green line) during MD simulation. (Colors in this figure are referred to the web version of this article.)

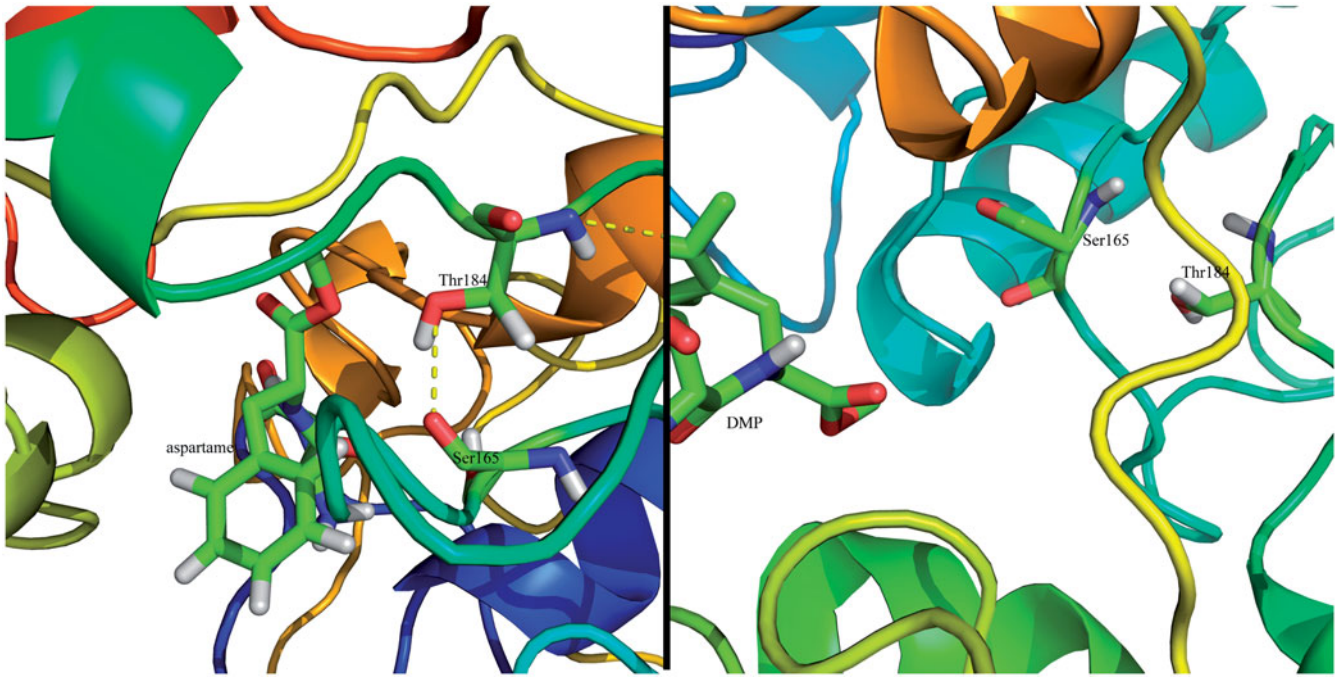

Figure 9. The computed binding mode of Ser165 with Thr184 in the binding site of T1R2 model in T1R2:aspartame (A) and T1R2:DMP (B) complexes. The hydrogen bonds are shown by the yellow dashed lines. (Colors in this figure are referred to the web version of this article.)

Table 3. Molecular energy terms for the T1R2:aspartame and T1R2:DMP complexes.

Energy (kcal/mol)	T1R2:aspartame complex	T1R2:DMP complex
ΔE_{vdw}	−151.380	−109.635
ΔE_{elect}	−136.582	−82.218
ΔE_{solv}	215.904	164.286
ΔE_{SASA}	−14.482	−12.043
$\Delta G_{binding}$	−86.539	−39.610

vdw, van der Waals; elect, electrostatic; solv, polar solvation; SASA, solvent-accessible surface area.

experiments demonstrated that DMP and DMT in place of native Phe in aspartame gave tasteless compounds. To further explore this result, a receptor model was built by homology in order to gain information about the binding mode of two aspartame models, and their lack to stimulate efficiently the sweet receptors (T1R2). Our data indicated that both phenylalanine-constrained surrogates, once inserted in the backbone of aspartame, deeply modify the binding mode at the T1R2 receptor model. In particular, by a comparison of the RMSD obtained by molecular dynamics simulations with of the aspartame derivatives bound to the receptor model, it is clear that native aspartame binds to the receptor in a unique way. We further confirmed our findings by RSM fluctuation of residues during MD simulation and more confirmations of these results were gained by measuring the distance changes between the ε nitrogen atom of Lys60 and oxygen of Ile306 in free T1R2, T1R2 complexed to aspartame and T1R2 complexed to DMP during MD simulation. Molecular docking also gave different binding properties for aspartame and its DMP analogue. The computed binding modes of Ser165 with Thr184 in the binding site of T1R2 model are very different in T1R2 complexed with aspartame and T1R2 complexed with DMP. Also 2D Roesy experiments were carried out. All those data are consistent with the hypothesis that the substitution of the native Phe of aspartame with conformational constrained residues such as DMP or DMT changes the conformational and stereo-electronic properties of aspartame. The overall 3D shape and conformational changes do not consent to the proposed molecules to correctly positioning in the binding pocket of the receptor, with a final lack of the signal transduction.

Declaration of interest

The authors report that they have no conflicts of interest.

References

1. Butchko HH, Stargel WW, Comer CP, et al. Aspartame: review of safety. Regul Toxicol Pharmacol 2002;35:S1–93.
2. Laffitte A, Neiers F, Briand L. Functional roles of the sweet taste receptor in oral and extraoral tissues. Curr Opin Clin Nutr Metab Care 2014;17:379–85.
3. Sigoillot M, Brockhoff A, Meyerhof W, Briand L. Sweet-taste-suppressing compounds: current knowledge and perspectives of application 2012;96:619–30.
4. Avenoza A, Parísa M, Peregrina JM, et al. Aspartame analogues containing 1-amino-2-phenylcyclohexanecarboxylic acids (c6Phe). Tetrahedron 2002;58:4899–905.
5. Formaggio F, Crisma M, Valle G. Conformationally restricted analogues of anti-aspartame-type sweeteners. J Chem Soc Perkin Trans 2 1992;2:1945–50.
6. Walters DE, Prakash I, Desai N. Active conformations of neotame and other high-potency sweeteners. J Med Chem 2000;43:1242–5.
7. Hruby VJ, Cai M. Design of peptide and peptidomimetic ligands with novel pharmacological activity profiles. Annu Rev Pharmacol Toxicol 2013;53:557–80.
8. Li T, Shiotani K, Miyazaki A, et al. Bifunctional [2′,6′-dimethyl-L-tyrosine[1]]endomorphin 2 analogues substituted at position 3 with alkylated phenylalanine derivatives yield potent mixed μ-agonist/δ-antagonist and dual μ-agonist/δ-agonist opioid ligands. J Med Chem 2007;50:2753–66.
9. Harrison BA, Pasternak GW, Verdine GL. 2,6-Dimethyltyrosine analogues of a stereodiversified ligand library: highly potent, selective, non-peptidic μ opioid receptor agonists. J Med Chem 2003;46:677–80.
10. Stefanucci A, Pinnen F, Feliciani F, et al. Conformationally constrained histidines in the design of peptidomimetics: strategies for the χ-space control. Int J Mol Sci 2011;12:2853–90.
11. Torino D, Mollica A, Pinnen F, et al. Synthesis and evaluation of new endomorphin analogues modified at the Pro[2] residue. Bioorg Med Chem Lett 2009;19:4115–18.

12. Torino D, Mollica A, Pinnen F, et al. Synthesis and evaluation of new endomorphin-2 analogues containing (Z)-α,β-Didehydrophenylalanine (Δ^{Z}Phe) residue. J Med Chem 2010; 53:4550–4.
13. Mollica A, Feliciani F, Stefanucci A, et al. N-(tert)-butyloxycarbonyl)-beta,beta-cyclopentyl-cysteine (acetamidomethyl)-methyl ester for synthesis of novel peptidomimetic derivatives. Protein Pept Lett 2010;17:925–9.
14. Karoyan P, Sagan S, Lequin O, et al. Targ Heter Sys 2005;8:216–73.
15. Zhang F, Klebansky B, Fine RM, et al. Molecular mechanism of the sweet taste enhancers. Proc Nat Acad Sci USA 2010;107: 4752–7.
16. (a) Mollica A, Pinnen F, Azzurra S, Costante R. The evolution of peptide synthesis: from early days to small molecular machines. Curr Bioact Comp 2013;9:184–202. (b) Mollica A, Paglialunga Paradisi M, Torino D, et al. Hybrid α/β-peptides: For–Met–Leu–Phe–OMe analogues containing geminally disubstituted β2,2- and β3,3-amino acids at the central position. Amino Acids 2006;30:453–9.
17. Dörrich S, Falgner S, Schweeberg S, et al. Silicon-containing dipeptidic aspartame and neotame analogues. Organometallics 2012; 31:5903–17.
18. Muto T, Tsuchiya D, Morikawa K, Jingami H. Structures of the extracellular regions of the group II/III metabotropic glutamate receptors. Proc Nat Acad Sci USA 2007;104:3759–64.
19. Larkin MA, Blackshields G, Brown NP, et al. Clustal W and Clustal X version 2.0. Bioinformatics 2007;23:2947–8.
20. McWilliam H, Li W, Uludag M, et al. Analysis tool web services from the EMBL-EBI. Nucleic Acids Res 2013;41:W597–600.
21. Shen MY, Sali A. Statistical potential for assessment and prediction of protein structures. Prot Sci 2006;15:2507–24.
22. Van Der Spoel D, Lindahl E, Hess B, et al. GROMACS: fast, flexible, and free. J Comp Chem 2005;26:1701–18.
23. Laskowski RA, MacArthur MW, Moss DS, Thornton JM. {PROCHECK}: a program to check the stereochemical quality of protein structures. J Appl Cryst 1993;26:283–91.
24. Trott O, Olson AJ. AutoDock Vina: improving the speed and accuracy of docking with a new scoring function, efficient optimization, and multithreading. J Comput Chem 2010;31:455–61.
25. Mirzaie S, Fathi F, Hakhamaneshi MS, et al. Combined 3D-QSAR modeling and molecular docking study on multi-acting quinazoline derivatives as HER2 kinase inhibitors. EXCLI J 2013;12:130–43.
26. Schuttelkopf AW, van Aalten DM. PRODRG: a tool for high-throughput crystallography of protein-ligand complexes. Acta Cryst D, Biol Cryst 2004;60:1355–63.
27. Gasteiger J, Marsili M. Iterative partial equalization of orbital electronegativity-a rapid access to atomic charges. Tetrahedron 1980;36:3219–28.
28. Wang R, Lai L, Wang S. Further development and validation of empirical scoring functions for structure-based binding affinity prediction. J Comput-aided Mol Des 2002;16:11–26.
29. Bas DC, Rogers DM, Jensen JH. Very fast prediction and rationalization of pKa values for protein-ligand complexes. Proteins 2008;73:765–83.
30. Lemkul JA, Allen WJ, Bevan DR. Practical considerations for building GROMOS-compatible small-molecule topologies. J Chem Inf Mod 2010;50:2221–35.
31. Mirzaie S, Najafi K, Hakhamaneshi MS. Investigation for antimicrobial resistance-modulating activity of diethyl malate and 1-methyl malate against beta-lactamase class A from *Bacillus licheniformis* by molecular dynamics, *in vitro* and *in vivo* studies. J Biomol Struct Dyn 2015;33:1016–26.
32. Berendsen HJC, Postma JPM, van Gunsteren WF, et al. Molecular dynamics with coupling to an external bath. J Chem Phys 1984;81: 3684–90.
33. Parrinello M, Rahman A. Polymorphic transitions in single crystals: a new molecular dynamics method. J Appl Phys 1981;52:7182–90.
34. Darden T, York D, Pedersen L. Particle mesh Ewald: an $N \log(N)$ method for Ewald sums in large systems. J Chem Phys 1993;98: 10089–92.
35. Hess B, Bekker H, Berendsen HJC, Fraaije JGEM. LINCS: a linear constraint solver for molecular simulations. J Comput Chem 1997; 18:1463–72.
36. Kumari R, Kumar R, Lynn A. g_mmpbsa – a GROMACS tool for high-throughput MM-PBSA calculations. J Chem Inf Model 2014; 54:1951–62.
37. Mollica A, Feliciani F, Stefanucci A, et al. Synthesis and biological evaluation of new active For–Met–Leu–Phe–OMe analogues containing *para*-substituted Phe residues. J Pept Sci 2012;18:418–26.
38. Kunishima N, Shimada Y, Tsuji Y, et al. Structural basis of glutamate recognition by a dimeric metabotropic glutamate receptor. Nature 2000;407:971–7.
39. Tsuchiya D, Kunishima N, Kamiya N, et al. Structural views of the ligand-binding cores of a metabotropic glutamate receptor complexed with an antagonist and both glutamate and Gd3+. Proc Nat Acad Sci USA 2002;99:2660–5.
40. Gundampati RK, Chikati R, Kumari M, et al. Protein–protein docking on molecular models of *Aspergillus niger* RNase and human actin: novel target for anticancer therapeutics. J Mol Mod 2012;18: 653–62.
41. Cui M, Jiang P, Maillet E, et al. The heterodimeric sweet taste receptor has multiple potential ligand binding sites. Curr Pharm Des 2006;12:4591–600.
42. Assadi-Porter FM, Tonelli M, Maillet EL, et al. Interactions between the human sweet-sensing T1R2-T1R3 receptor and sweeteners detected by saturation transfer difference NMR spectroscopy. Biochim Biophys Acta 2010;1798:82–6.
43. Acher FC, Selvam C, Pin JP, et al. A critical pocket close to the glutamate binding site of mGlu receptors opens new possibilities for agonist design. Neuropharmacology 2011;60:102–7.
44. Parenti MD, Rastelli G. Advances and applications of binding affinity prediction methods in drug discovery. Biotechnol Adv 2012; 30:244–50.
45. Venken T, Krnavek D, Munch J, et al. An optimized MM/PBSA virtual screening approach applied to an HIV-1 gp41 fusion peptide inhibitor. Proteins 2011;79:3221–35.
46. Barakat KH, Jordheim LP, Perez-Pineiro R, et al. Virtual screening and biological evaluation of inhibitors targeting the XPA-ERCC1 interaction. PloS One 2012;7:e51329.

Supplementary material available online
Supplemental material.